AIMS Mathematics, 11(4): 11559–11579.
DOI: 10.3934/math.2026476
Received: 27 February 2026
Revised: 02 April 2026
Accepted: 10 April 2026
Published: 27 April 2026

https://www.aimspress.com/journal/Math

Research article

Hopf bifurcation analysis in a reaction-diffusion-advection model with strong Allee effect and delay

Yuying Liu[1,2,*], **and Xin Wei**[3]

[1] School of Mathematics, China University of Mining and Technology, Xuzhou, Jiangsu 221116, China
[2] Jiangsu Center for Applied Mathematics at CUMT, Xuzhou, Jiangsu 221116, China
[3] School of Mathematical Sciences, Heilongjiang University, Harbin, Heilongjiang 150001, China

* **Correspondence:** Email: liuyuying@cumt.edu.cn.

Abstract: This paper investigates a delayed population model incorporating advection and strong Allee effect. First, we prove the well-posedness of the solutions in the model. The effect of the advection rate on the dynamics of the population is examined. Analysis indicates that under the given conditions, a larger advection rate can stabilize the equilibrium of the model. Second, by adopting delay as the varying parameter, the Hopf bifurcation of the model is studied. Third, the normal form in the vicinity of the Hopf bifurcation singularity is calculated by adopting a weighted inner product. The reliability of the conclusion is then verified by means of the numerical simulations. Research shows that under specific conditions, there exists a sequence of Hopf bifurcation singularities in the system.

Keywords: Allee effect; reaction-diffusion-advection; normal form; Hopf bifurcation
Mathematics Subject Classification: 35K57, 37G15

1. Introduction

In 1859, thirteen European rabbits (Oryctolagus cuniculus) were introduced to Australia. Subsequently, they expanded their range at an unprecedented rate, exceeding 100 kilometers per year, establishing themselves as one of the fastest-spreading invasive mammal species globally [1]. The ensuing overpopulation has driven significant environmental harm, characterized by vegetation overgrazing that induces soil degradation and disease transmission that threatens native wildlife with extinction. These consequences have imposed a heavy economic burden on Australia.

Biological invasion poses significant ecological risks. When a new species is introduced into a specific region, is it inevitably able to establish a stable, long-term population? The answer is no. For instance, countries including Australia once attempted to introduce ferrets, the natural predators of

European rabbits, to control the overpopulation of rabbits. However, the introduced ferrets ultimately failed to establish a sustainable population in Australia [2]. This case demonstrates that invasion is not always successful. In fact, for many social species, to successfully colonize a novel environment, the initial population size must be sufficiently large to withstand the impacts of environmental factors on population abundance.

To explore the dynamics of the invasive species, we will perform an analysis by means of biomathematical models. In ecosystems, the logistic growth rate serves as a fundamental tool for depicting population expansion and effectively captures the effect of intraspecific competition. The logistic growth rate describes the fact that when population density increases, the growth rate declines. In 1931, the ecologist Allee observed that in social populations, the intrinsic growth rate decreases below a critical population threshold [3]. This phenomenon, known as the strong Allee effect, has since been extensively studied in subsequent ecological models [4–6]. Given that the successful colonization of invasive social species depends on a sufficiently large initial population size (as demonstrated by the ferret introduction case in Australia), the strong Allee growth model is more biologically realistic for our study.

The strong Allee effect reveals the phenomenon that the coexistence of conspecifics brings survival benefits to individual animals. A model incorporating a strong Allee effect exhibits a growth rate influenced by cooperative and competitive interactions among individuals [7, 8]. Numerical evidence substantiates that a critical density threshold is a defining characteristic of the strong Allee effect, and population density below this threshold cannot guarantee long-term persistence [9].

Time delays are ubiquitous in the study of population dynamics [10–12]. Social populations often exhibit a lagged feedback effect in resource consumption: The high-density resource consumption of a population at time $t - \tau$ will not lead to a significant resource shortage until a time interval of τ has elapsed, which then exerts an inhibitory effect on the population growth rate at time t. Incorporating this feedback effect into the strong Allee growth model yields

$$\dot{u} = ru(u - b)\left[1 - \frac{u(t - \tau)}{K}\right].$$

We should emphasize that in the study of population dynamics within bounded domains, it is found that population density varies with spatial location. Individuals undergo both random dispersal and directed movement [13, 14]. Diffusion and advection enable the investigation of the spatiotemporal population distribution [15]. Whereas random diffusion is often associated with the spatial heterogeneity, how does directional movement affect population dynamics? Based on these considerations, this paper investigates the following model defined on a bounded region:

$$\begin{cases} \frac{\partial u(x,t)}{\partial t} = d\frac{\partial^2 u(x,t)}{\partial x^2} - \alpha\frac{\partial u(x,t)}{\partial x} + ru(x,t)[u(x,t) - 1][1 - u(x,t-\tau)/K], & x \in (0,L), t \geq 0, \\ du_x(0,t) - \alpha u(0,t) = -\alpha K, \;\; u(L,t) = K, & t \geq 0, \end{cases} \tag{1.1}$$

where $u(x,t)$ stands for the population density at the spatiotemporal point (x,t), d denotes the diffusion rate, α denotes the advection rate, the parameter $K > 1$ represents the carrying capacity, the Allee threshold is rescaled to 1, L denotes the region range, and τ represents the time-delayed effect of intraspecific competition on population growth. We should emphasize that the boundary conditions are set as follows: The boundary condition at $x = 0$ is defined as a "transitional boundary" that accounts for the dynamic equilibrium between diffusion and advection, aiming to prevent the

population from density instability caused by unconstrained diffusion and directional migration; the boundary $x = L$ is designed as A source boundary with stable population supplementation, ensuring that the population density remains in a saturated state. The boundary conditions are the modified no-flux/hostile (NF/H) boundary conditions [16]; these boundary conditions are commonly used in studying the distribution and migration of species in rivers. If Model (1.1) contains no advection term, the corresponding theoretical analysis method can be referred to in [9].

In ecological systems, the stability and periodic oscillation of population sizes are crucial for the long-term persistence of populations [17–19]. Bifurcation analysis is one of the classical methods for studying population oscillations, and numerous scholars have conducted relevant research in this field [20–22]. In recent years, scholars have also investigated the high-codimension bifurcation problems in reaction-diffusion equation models [23]. Reference [24] explored the Hopf-Hopf bifurcation of a nonlocal competitive population model. Reference [25] investigated the degenerate Turing-Hopf bifurcation of reaction-diffusion equations and verified the results by applying them to an autocatalysis model. These theoretical studies have enriched the bifurcation theory of reaction-diffusion equations. However, studies on the bifurcation theory of population models with advection and diffusion are relatively scarce. Most existing studies focus on abstract theoretical frameworks, and few have performed specific calculations of normal forms.

Recently, several studies have focused on the dynamics of models with advection. Numerical evidence is provided for the existence of Hopf singularity in a competition model with advection [26]. A rigorous analysis of spatially nonhomogeneous solutions for an advection-diffusion model that evolves nonlocal delay was presented in [27]. Unlike existing studies, this paper aims to theoretically investigate the Hopf bifurcation in an advection-diffusion model (1.1) and derive the normal form that determines the properties of the bifurcation.

Various analytical approaches are available for the study of advection-diffusion models. In our work, we draw support from operator theory and observe that the eigenfunctions of the linear operator under consideration fail to form an orthogonal basis under the L^2 inner product. However, these eigenfunctions become orthogonal by introducing a suitably defined weighted inner product. We emphasize two points of this work: first, we compute the normal forms in a delayed advection-diffusion model with a weighted inner product; Second, Hopf bifurcation is proved both theoretically and numerically. Additionally, the normal form here can be extended to other advection models.

The structure of this paper is outlined below. In Section 2, the analysis of the equilibrium and Hopf bifurcations are conducted. In Section 3, the properties of the resulting periodic solutions are analyzed. Finally, simulations in Section 4 validate the theoretical findings.

2. Stability and bifurcations analysis

By direct calculation, Model (1.1) has an equilibrium $u_* = K$. For convenience in calculations, let $\tilde{u} = u - K$, so that (1.1) becomes

$$\begin{cases} \frac{\partial \tilde{u}(x,t)}{\partial t} = d\frac{\partial^2 \tilde{u}(x,t)}{\partial x^2} - \alpha\frac{\partial \tilde{u}(x,t)}{\partial x} - \frac{r}{K}[\tilde{u}(x,t)+K][\tilde{u}(x,t)+K-1]\tilde{u}(x,t-\tau), & x \in (0,L), t \geq 0, \\ d\tilde{u}_x(0,t) - \alpha\tilde{u}(0,t) = 0, \ \ \tilde{u}(L,t) = 0, & t \geq 0. \end{cases} \tag{2.1}$$

Obviously, the dynamical properties of $u_* = K$ in (1.1) are equivalent to those of $\tilde{u} = 0$ in (2.1). As to the stability of $\tilde{u} = 0$ in (2.1), we will first analyze the distribution of eigenvalues in the linearized

equation corresponding to the model (2.1) at the origin. In the rest, we remove the tilde on $\tilde{u}$ in (2.1) to simplify the symbols. For clarity, we rewrite Eq (2.1) as follows.

$$\begin{cases} \frac{\partial u(x,t)}{\partial t} = d\frac{\partial^2 u(x,t)}{\partial x^2} - \alpha\frac{\partial u(x,t)}{\partial x} - \frac{r}{K}[u(x,t)+K][u(x,t)+K-1]u(x,t-\tau), & x \in (0,L), t \geq 0, \\ du_x(0,t) - \alpha u(0,t) = 0, \quad u(L,t) = 0, & t \geq 0. \end{cases} \tag{2.2}$$

To simplify notation, we define the following spaces:

$$X := \left\{\phi \in H^2(0,L) | \, d\phi'(0) - \alpha\phi(0) = 0, \quad \phi(L) = 0\right\},$$

$Y = L^2((0,L))$, $C = C([-\tau, 0], X)$, and $C = C([-1, 0], X)$. The space $S_{\mathbb{C}} := S \oplus \mathrm{i}S = \{s_1 + \mathrm{i}s_2 \mid s_1, s_2 \in S\}$ is defined as the complexification of S.

Denote

$$\eta_t(\theta)(x) := u(x, t+\theta), \quad \forall \theta \in [-\tau, 0], \ x \in (0, L),$$

where $\eta_t \in C$ denotes the state of System (2.2), encoding both current and historical information of u over $[t-\tau, t]$. As for the well-posedness of the system's solutions, we develop the following theorem.

Theorem 2.1. *For any initial delay segment $\eta_0 \in C([-\tau, 0], X)$, that is, $\eta_0(\theta) = u_0(x, \theta)$ satisfies $\eta_0(\theta) \in X$ for all $\theta \in [-\tau, 0]$, there exists a unique solution $\eta_t \in C^1([0, \infty); C)$ to the abstract delayed differential equation (DDE) corresponding to System* (2.2)*. Therefore, the unique solution $u(x, t) = \eta_t(0)(x)$ exists in Eq* (2.2) *which satisfies*

$$u \in C([0, \infty) \times [0, L]) \cap C^1((0, \infty); X) \cap L^\infty((0, \infty); X).$$

Proof. First, we recast System (2.2) as an abstract DDE in the state space C. Define the linear operator $\tilde{A} : D(\tilde{A}) \subset C \to C$ as

$$\tilde{A}\eta(\theta) := \frac{d\eta}{d\theta}(\theta), \theta \in (-\tau, 0), \eta \in D(\tilde{A}),$$

with

$$D(\tilde{A}) := \{\eta \in C^1([-\tau, 0], Y) \mid \eta(0) \in X, \ d\eta'(0) - \alpha\eta(0) = 0, \ \eta(\theta) \in X, \forall \theta \in [-\tau, 0]\}.$$

Then, we have

$$\begin{aligned} \langle \tilde{A}v, v\rangle &= \int_0^L \tilde{A}v \cdot v \mathrm{d}x \\ &= \int_0^L (dv'' - av')v \mathrm{d}x \\ &= -d\int_0^L v'^2 \mathrm{d}x - \frac{1}{2}av^2(0) < 0, \end{aligned}$$

which indicates that $\tilde{A}$ is dissipative. For $\tilde{\lambda} > 0$ and $\tilde{f} \in Y$, the equation $\tilde{\lambda}v - \tilde{A}v = \tilde{f}$ has only one solution, $v \in \mathcal{D}(\tilde{A})$, under the NF/H boundary condition. What's more, we note that the densely defined closed operator $\tilde{A}$ is capable of generating the corresponding C_0-contraction semigroup $T(t)$ on the space C.

For $\eta \in C$, define the nonlinear mapping $\tilde{F} : C \to C$ as

$$\tilde{F}(\eta)(0) := -\frac{r}{K}[\eta(0) + K][\eta(0) + K - 1]\eta(-\tau),$$

and

$$\tilde{F}(\eta)(\theta) := 0,\ \theta \in (-\tau, 0).$$

For any $\tilde{M} > 0$, $\eta_1, \eta_2 \in Y$ with $\|\eta_i\| \leq \tilde{M}$, we can prove that

$$|\tilde{F}(\eta_1) - \tilde{F}(\eta_2)| \leq L(\tilde{M})\|\eta_1 - \eta_2\|,$$

where $L(\tilde{M}) = \frac{r}{K}[2\tilde{M}^2 + 2(2K-1)\tilde{M} + K(K-1)]$. Thus, $\tilde{F}$ is locally Lipschitz continuous on $C([-\tau, 0], X)$.

Now, the abstract DDE corresponding to System (2.2) reads

$$\begin{cases} \frac{d}{dt}\eta_t = \tilde{A}\eta_t(\theta) + \tilde{F}(\eta_t), \\ \eta_0(\theta) = u_0(x, \theta). \end{cases} \tag{2.3}$$

Define a sequence $\{\eta_t^{(n)}\}$ as

$$\begin{cases} \eta_t^{(0)} = \eta_0, \\ \eta_t^{(n)} = T(t)\eta_0(0) + \int_0^t T(t-s)\tilde{F}(\eta_s^{(n-1)})ds, \quad t \in [0, T]. \end{cases}$$

For $T < 1/L(\tilde{M})$, the sequence $\{\eta_t^{(n)}\}$ converges uniformly in $C([-\tau, 0], X)$. Suppose that $\eta_t^{(a)}$ and $\eta_t^{(b)}$ are two solutions of (2.3), then

$$\|\eta_t^{(a)} - \eta_t^{(b)}\| \leq L(\tilde{M}) \int_0^t \|\eta_s^{(a)} - \eta_s^{(b)}\|ds.$$

Based on Grönwall's inequality, we can conclude $\eta_t^{(a)} = \eta_t^{(b)}$.

Therefore, Eq (2.3) admits one unique solution in $C([-\tau, 0], X)$, and thus, System (2.2) has only one solution, $u(x, t) \in C([0, T] \times [0, L]) \cap C^1([0, T]; X) \cap L^\infty([0, T]; X)$. By expanding the local solution to $[0, \infty)$, we can finally conclude that the solution to System (2.2) which is compatible with the boundary conditions exists and is unique. □

Now, we will examine the stability of the zero solution in System (2.2). Linearizing (2.2) at the origin reads

$$\begin{cases} \frac{\partial u(x,t)}{\partial t} = d\frac{\partial^2 u(x,t)}{\partial x^2} - \alpha\frac{\partial u(x,t)}{\partial x} - r(K-1)u(x, t-\tau), \quad x \in (0, L), t \geq 0, \\ du_x(0, t) - \alpha u(0, t) = 0,\ \ u(L, t) = 0, \quad t \geq 0. \end{cases} \tag{2.4}$$

By direct calculation, the eigenvalues associated with the subsequent problem

$$\begin{cases} d\frac{\partial^2 \varphi(x)}{\partial x^2} - \alpha\frac{\partial \varphi(x)}{\partial x} = -\mu\varphi(x), \\ d\varphi'(0) - \alpha\varphi(0) = 0, \quad \varphi(L) = 0, \end{cases} \tag{2.5}$$

can be expressed as $\{\mu_n\}_{n\geq 1}$, where $\alpha^2/(4d) < \mu_n < \mu_{n+1}$ and

$$\tan\frac{\sqrt{4d\mu_n - \alpha^2}}{2d}L + \frac{\sqrt{4d\mu_n - \alpha^2}}{\alpha} = 0. \tag{2.6}$$

The associated eigenfunction of μ_n is

$$\varphi_n = e^{\frac{\alpha}{2d}x}(\sqrt{4d\mu_n - \alpha^2}\cos\frac{\sqrt{4d\mu_n - \alpha^2}}{2d}x + \alpha\sin\frac{\sqrt{4d\mu_n - \alpha^2}}{2d}x), n = 1, 2, 3, \ldots$$

Obviously, the explicit expression of μ_n in Eq (2.6) cannot be derived explicitly, however, the monotonicity of μ_n with respect to the parameters α and d can be established, and the conclusions are as follows.

Lemma 2.2. *When regarding the eigenvalue μ_n ($n = 1, 2, \ldots$) in Eq* (2.6) *as an implicit function of the parameter α, μ_n is a strictly increasing function of α, that is, $\mu_n'(\alpha) > 0$.*

Proof. Define the implicit function

$$F(\mu_n, \alpha) = \tan\left(\frac{\sqrt{4d\mu_n - \alpha^2}\cdot L}{2d}\right) + \frac{\sqrt{4d\mu_n - \alpha^2}}{\alpha} = 0.$$

From the implicit function theorem, $\mu_n'(\alpha)$ exists and satisfies:

$$\frac{d\mu_n}{d\alpha} = -\frac{\partial F/\partial\alpha}{\partial F/\partial\mu_n}.$$

By direct calculation, we have

$$\frac{\partial F}{\partial\mu_n} = \frac{L\sec^2\left(\frac{\sqrt{4d\mu_n-\alpha^2}\cdot L}{2d}\right)}{\sqrt{4d\mu_n - \alpha^2}} + \frac{2d}{\alpha\sqrt{4d\mu_n - \alpha^2}} > 0.$$

Thus, the sign of the denominator $\partial F/\partial\mu_n$ is positive. Additionally,

$$\frac{\partial F}{\partial\alpha} = -\frac{\alpha L\sec^2\left(\frac{\sqrt{4d\mu_n-\alpha^2}\cdot L}{2d}\right)}{2d\sqrt{4d\mu_n - \alpha^2}} - \frac{4d\mu_n}{\alpha^2\sqrt{4d\mu_n - \alpha^2}} < 0,$$

which means that the numerator $\partial F/\partial\alpha$ is negative. Thus, $\mu_n'(\alpha) > 0$, which proves that μ_n is strictly increasing with respect to α. □

This lemma reveals the quantitative relationship between the advection rate α and the eigenvalues μ_n. Specifically, an increase in α induces a monotonic rise in μ_n.

We specify the characteristic equations associated with (2.4) in the following:

$$\lambda + \mu_n + r(K-1)e^{-\lambda\tau} = 0, \quad n = 1, 2, \ldots \tag{2.7}$$

When $\tau = 0$, the roots of (2.7) take the form

$$\lambda_n = -\mu_n - r(K-1), \quad n = 1, 2, \ldots \tag{2.8}$$

Apparently, all roots of (2.7) are negative. Therefore, $u_* = K$ is stable for $\tau = 0$.

Selecting τ as the bifurcation parameter, we study the existence of Hopf singularity for System (1.1). Let $\tau > 0$ such that Eq (2.7) has a purely imaginary eigenvalue $\pm i\omega(\omega > 0)$. Since $i\omega$ satisfies Eq (2.7), it follows that

$$r(K-1)(\cos\omega\tau - i\sin\omega\tau) + \mu_n + i\omega = 0. \tag{2.9}$$

Decomposing Eq (2.9) into its real and imaginary components, we obatin

$$\begin{cases} r(K-1)\cos\omega\tau = -\mu_n, \\ r(K-1)\sin\omega\tau = \omega. \end{cases} \tag{2.10}$$

It follows from (2.10) that

$$\omega^2 + \mu_n^2 = r^2(K-1)^2. \tag{2.11}$$

Thus, the roots of Eq (2.11) are given by

$$\omega = \sqrt{r^2(K-1)^2 - \mu_n^2} := \omega_n. \tag{2.12}$$

Clearly, (2.12) does not make sense when $\mu_n \geq r(K-1)$, which means that (2.7) has no purely imaginary roots if

$$\mu_1 \geq r(K-1). \tag{2.13}$$

Therefore, if $\min_{n\geq 1}\{\mu_n\} = \mu_1 < r(K-1)$, an integer $n_0 > 1$ exists such that Eq (2.12) is well-defined for $1 \leq n < n_0$ and undefined for $n \geq n_0$. Since all roots of (2.7) have negative real parts at $\tau = 0$, the following theorem holds.

Theorem 2.3. *For System* (1.1)*, we can deduce that*

(i) if $\mu_1 \geq r(K-1)$, then the spectrum of Eq (2.7) *is confined to the left half-plane of the complex plane for any $\tau > 0$;*
(ii) if $\mu_1 < r(K-1)$, an integer $n_0 > 1$ exists such that (2.12) *is well-defined for $1 \leq n < n_0$ and undefined for $n \geq n_0$.*

Assume that

$$(H_1) \quad \mu_1 < r(K-1).$$

Under the hypothesis (H_1), we define an integer $n_0 > 1$ with the following property: Eq (2.12) is well-defined for all n satisfying $1 \leq n < n_0$; however, it is ill-defined for all $n \geq n_0$. From Eq (2.10), we have

$$\tau_n^{(j)} = \frac{1}{\omega_n}\arccos\frac{-\mu_n}{r(K-1)} + \frac{2j\pi}{\omega_n}, n = 1, 2, \ldots, n_0 - 1, j = 0, 1, \ldots \tag{2.14}$$

Indeed, since $\cos(\omega_n\tau_n^{(j)}) < 0$, and $\sin(\omega_n\tau_n^{(j)}) > 0$, it indicates that $\omega_n\tau_n^{(j)} \in (\pi/2, \pi)$.

Lemma 2.4. *Suppose (H_1) holds. Then, for all $\tau_n^{(j)}$ such that Eq* (2.12) *is well-defined, we have*

$$\min_{1\leq n<n_0} \tau_n^{(j)} = \tau_1^{(0)}.$$

This lemma can be deduced from the monotone property of the arccosine function. For simplicity, we denote $\tau_* := \tau_1^{(0)}$ in the rest of this paper.

Through the analysis of the linearized system, we have derived the characteristic equations (2.7). These equations clearly reveal the structural relationship among parameters in Model (1.1): The diffusion coefficient d affects the eigenvalue through the additive term μ_n, and the time delay τ is introduced nonlinearly via the multiplicative exponential term $e^{-\lambda\tau}$. These two terms are mathematically separated in structure, which fundamentally leads to the decoupled behavior between the diffusion coefficient d and the delay τ in triggering Hopf bifurcations.

Additionally, since the expression for the Hopf bifurcation threshold $\tau_n^{(j)}$ includes ω_n and μ_n, both of which are functions of the diffusion coefficient d. Notice that for a fixed d, $\tau_{n+1}^{(j)} < \tau_n^{(j)}$ holds. The numerical results in the Figure 1 directly reflect the relationship between d and $\tau_n^{(j)}$.

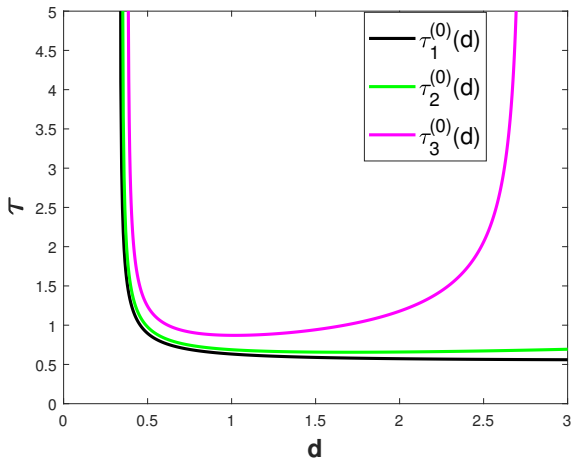

Figure 1. Several Hopf bifurcation curves on the d-τ plane, with $r = 1$, $K = 4$, $L = 8$, $\alpha = 2$.

To investigate whether the simultaneous variation of d and τ can give rise to spatiotemporal periodic phenomena in the system (1.1), we provide the following necessary conditions for the existence of Hopf-Hopf bifurcation, Turing-Hopf bifurcation, Bogdanov-Takens bifurcation and Bautin bifurcation. For precise definitions of these bifurcations, we refer the reader to [29] and [30].

Proposition 1. *For System* (1.1)*, if a Hopf-Hopf bifurcation arises at E_*, then Eq* (2.7) *admits two pairs of conjugate imaginary roots, with real parts of these eigenvalues having nonzero derivatives with respect to the parameter. If the Turing-Hopf bifurcation occurs at E_*, then Eq* (2.7) *exhibits one simple zero root and one pair of conjugate purely imaginary roots, and the real parts of the eigenvalues have a nonzero derivative with respect to the parameters.*

Proposition 2. *For System* (1.1)*, if a Bogdanov-Takens bifurcation exists at E_*, then Eq* (2.7) *has a zero eigenvalue of (algebraic) multiplicity two. If the Bautin bifurcation exists, then Eq* (2.7) *has a pair of conjugate imaginary roots, with the first Lyapunov coefficient equal to zero.*

Notably, for System (1.1), when the two parameters d and τ are varied simultaneously, if two distinct Hopf bifurcation curves intersect, the intersection point is precisely the Hopf-Hopf singularity; if a Hopf bifurcation curve intersects a zero-eigenvalue curve, the intersection point is precisely the Turing-Hopf bifurcation singularity.

By combining Lemma 2.4 with Propositions 1 and 2, we obtain the following result.

Lemma 2.5. *When considering the simultaneous variation of τ and d, the above analysis rules out Hopf–Hopf, Turing–Hopf, and Bogdanov–Takens bifurcations, whereas the possibility of a Bautin bifurcation cannot be excluded in System* (1.1).

By treating d as a variable and τ as a function, we consider the bifurcation curves $\tau = \tau_n^{(j)}(d)$. According to Lemma 2.4, it is impossible for two Hopf bifurcation curves to intersect at the boundary of the stable region within the $\tau - d$ plane. Besides, zero is not a root of Eq (2.7). Therefore, System (1.1) cannot undergo Hopf-Hopf, Turing-Hopf, or Bogdanov-Takens bifurcations. This is illustrated in Figure 1.

Remark 1. *Lemma 2.5 considers the existence of codimension-two bifurcations in System* (1.1) *when d and τ are taken as two varying parameters. If other pairs of parameters are considered as varying parameters, the existence of the corresponding codimension-two bifurcations also merits further investigation, and the conclusions may differ.*

It has been established that for $\tau = \tau_n^{(j)}$ (for $n = 1, 2, \ldots, n_0 - 1$, $j = 0, 1, \ldots$), the values of $\pm \mathrm{i}\omega_n$ constitute two roots of Eq (2.7). Let $\lambda(\tau)$ be a root of Eq (2.7), with

$$\mathrm{Re}\,\lambda\left(\tau_n^{(j)}\right) = 0 \ \text{ and } \ \mathrm{Im}\,\lambda\left(\tau_n^{(j)}\right) = \omega_n,$$

the following lemma can be deduced.

Lemma 2.6. *Suppose (H_1) holds. Then,* $\mathrm{Re}\,\lambda'\left(\tau_n^{(j)}\right) > 0$.

Proof. The substitution of $\lambda(\tau)$ into Eq (2.7) is followed by differentiating two sides with respect to τ, thereby obtaining

$$\lambda' + r(K-1)e^{-\lambda\tau}(-\lambda'\tau - \lambda) = 0;$$

thus,

$$\left(\frac{\mathrm{d}\lambda}{\mathrm{d}\tau}\right)^{-1} = \frac{e^{\lambda\tau}}{\lambda r(K-1)} - \frac{\tau}{\lambda}.$$

When $\tau = \tau_n^{(j)}$, we know that $\lambda = \mathrm{i}\omega_n$; thus,

$$\begin{aligned}
\mathrm{Re}\left(\frac{\mathrm{d}\lambda}{\mathrm{d}\tau}\right)^{-1}\Bigg|_{\tau=\tau_{n,j}} &= \mathrm{Re}\left[\frac{e^{\lambda\tau}}{\lambda r(K-1)} - \frac{\tau}{\lambda}\right]\Bigg|_{\tau=\tau_{n,j}} \\
&= \mathrm{Re}\left[\frac{1}{-\lambda^2 - \lambda\mu_n} - \frac{\tau}{\lambda}\right]\Bigg|_{\lambda=\mathrm{i}\omega_n} \\
&= \mathrm{Re}\left[\frac{1}{\omega^2 - \mathrm{i}\omega\mu_n}\right]\Bigg|_{\lambda=\mathrm{i}\omega_n} \\
&= \frac{1}{\omega^2 + \mu_n^2} > 0.
\end{aligned}$$

Since

$$\mathrm{Sign}\left[\mathrm{Re}\,\lambda'\left(\tau_n^{(j)}\right)\right] = \mathrm{Sign}\left[\mathrm{Re}\left(\frac{\mathrm{d}\lambda}{\mathrm{d}\tau}\right)^{-1}\Bigg|_{\tau=\tau_n^{(j)}}\right] > 0,$$

the derivations presented above adequately validate the conclusion, thus finalizing the proof. □

The root distribution of Eq (2.7) can be summarized as follows.

Lemma 2.7. *Under Assumption* (H_1)*, the roots of Eq* (2.7) *all possess negative real parts in the case of* $\tau < \tau_*$*. When* τ *equals* τ_**, a pair of imaginary roots* $\pm i\omega_n$ *emerges, whereas others retain negative real parts. Once* τ *exceeds* τ_**, no fewer than two roots acquire positive real parts.*

Lemmas 2.4–2.7 enable us to put forward the following theorem about the dynamical behaviors of Model (1.1).

Theorem 2.8. *The stability of* $u_* = K$ *depends on the parameters in System* (1.1)*.*

(i) If $\mu_1 \geq r(K-1)$*,* $u_* = K$ *possesses unconditional stability for all* $\tau \geq 0$*;*
(ii) If $\mu_1 < r(K-1)$*,* $u_* = K$ *is stable for* $\tau < \tau_*$ *and unstable for* $\tau > \tau_*$*; meanwhile, System* (1.1) *exhibits Hopf singularity at* $\tau = \tau_n^{(j)}, n = 1, 2, \ldots, n_0 - 1, j = 0, 1, 2, \ldots$

We can draw from Lemma 2.2 and Theorem 2.8 that when the advection rate increases with other parameters fixed, μ_1 increases monotonically. Consequently, the equilibrium $u_* = K$ in System (1.1) may switch from unstable to stable. This indicates that for System (1.1), a larger advection rate is more likely to stabilize the population.

3. Property of Hopf bifurcation

This section focuses on determining the properties of Hopf bifurcation at τ_*, employing the following variable transformation: $U(t) = u(\cdot, t) - u_*$, $s = \tau t, \tau = \tau_* + \mu$. Eq (2.2) can be written as

$$\frac{\mathrm{d}U(t)}{\mathrm{d}s} = d\tau_*\Delta U(s) - \alpha\tau_*\nabla U(s) + L_1U_s + F(U_s, \mu), \tag{3.1}$$

with $U_s \in C$,

$$\begin{aligned} L_1U_s =& -\tau_* r(K-1)U(s-1), \\ F(U_s, \mu) =& \mu\big[d\Delta U(s) - \alpha\nabla U(s) - r(K-1)U(s-1)\big] \\ & - (\tau_* + \mu)\big[\frac{r(2K-1)}{K}U(s)U(s-1) + \frac{r}{K}U^2(s)U(s-1)\big]. \end{aligned}$$

These transformations aim to translate the Hopf bifurcation point $\tau = \tau_*$ of the original system to $\mu = 0$, simplifying the calculation of normal forms near the critical singularity. For better understanding, we will denote s as t from now on. As established in the previous section, Hopf singularity occurs at the origin in System (2.2) when $\mu = 0$. Furthermore, in this critical case, the characteristic equations admit a conjugate pair of roots $\pm i\omega_1\tau_*$. Specifically, aside from this conjugate pair, other characteristic roots have negative real parts. Linearizing Eq (3.1) for $\mu = 0$ reads

$$\frac{\mathrm{d}U(t)}{\mathrm{d}t} = d\tau_*\Delta U(t) - \alpha\tau_*\nabla U(t) + L_1U_t. \tag{3.2}$$

Let $\mathcal{A}_0$ represents an infinitesimal generator corresponding to the solution semigroup of Eq (3.2). Then, we have

$$\mathcal{A}_0\Psi = \dot{\Psi},$$

$$\mathscr{D}(\mathcal{A}_0) = \left\{\Psi \in C_{\mathbb{C}} \cap C^1_{\mathbb{C}} : \Psi(0) \in X_{\mathbb{C}}, \dot{\Psi}(0) = d\tau_*\Delta\Psi(0) - \alpha\tau_*\nabla\Psi(0) - \tau_* r(K-1)\Psi(-1)\right\},$$

where

$$C^1_{\mathbb{C}} = C^1([-1, 0], X_{\mathbb{C}}).$$

With the aid of the following Banach space B_s consisting of continuous functions

$$\mathrm{B}_s := \{\psi \in C([-1, 0)) \text{ and } \lim_{\theta \to 0^-} \psi(\theta) \in Y_C\},$$

Eq (3.1) can be formulated in the form of an abstract differential equation:

$$\frac{\mathrm{d}U_t}{\mathrm{d}t} = \mathcal{A}_0 U_t + X_0 F(U_t, \mu), \tag{3.3}$$

where $X_0(\theta)$ is the product of the Dirac function and the 2nd-order identity matrix, i.e. $X_0(\theta) = \delta(\theta) I_2$, $\theta \in [-1, 0]$.

Due to the advection term $-\alpha \nabla U(t)$, the eigenfunctions of $\mathcal{A}_0$ do not form an orthogonal basis under the standard L^2 inner product. To construct an orthonormal basis for the center subspace, we introduce a weighted inner product, which is consistent with the advection-diffusion structure of the model. Therefore, the computation of normal forms requires the definition of a weighted inner product in the space $Y_{\mathbb{C}}$:

$$\langle u, v\rangle_1 = \int_0^L e^{-\frac{\alpha}{d}x} \overline{u}(x) v(x) dx \quad \text{for} \quad u, v \in Y_{\mathbb{C}}.$$

Here, the weight function is associated with the ratio of the advective rate to the diffusive rate. For $\alpha \geq 0$,

$$e^{-\frac{\alpha}{d}L} \langle u, v\rangle \leq \langle u, v\rangle_1 \leq \langle u, v\rangle,$$

and for $\alpha \leq 0$,

$$\langle u, v\rangle \leq \langle u, v\rangle_1 \leq e^{-\frac{\alpha}{d}L} \langle u, v\rangle.$$

Adopting the approach of [14], the formal duality $\langle\langle \cdot, \cdot \rangle\rangle$ is established in C with

$$\langle\langle \psi, \phi\rangle\rangle = \langle \psi(0), \phi(0)\rangle_1 - \tau_* r(K-1) \int_{-1}^{0} \langle \psi(s+1), \phi(s)\rangle_1 \mathrm{d}s, \tag{3.4}$$

for $\phi \in C_{\mathbb{C}}$ and $\psi \in C^*_{\mathbb{C}} := C([0, 1], Y_{\mathbb{C}})$. We remark that $\mathcal{A}^*$ is the formal adjoint operator of $\mathcal{A}_0$ if

$$\langle\langle \mathcal{A}^* \tilde{\Psi}, \Psi\rangle\rangle = \langle\langle \tilde{\Psi}, \mathcal{A}_0 \Psi\rangle\rangle$$

for any $\Psi \in \mathscr{D}(\mathcal{A}_0)$ and $\tilde{\Psi} \in \mathscr{D}(\mathcal{A}^*)$.

Definition 3.1. *We define the formal adjoint operator $\mathcal{A}^*$ as*

$$\mathcal{A}^* \tilde{\Psi}(s) = -\dot{\tilde{\Psi}}(s),$$

with the domain

$$\mathscr{D}(\mathcal{A}^*) = \left\{\tilde{\Psi} \in C^*_{\mathbb{C}} \cap (C^*_{\mathbb{C}})^1 : \tilde{\Psi}(0) \in X_{\mathbb{C}}, -\dot{\tilde{\Psi}}(0) = d\tau_* \Delta \tilde{\Psi}(0) - \alpha \tau_* \nabla \tilde{\Psi}(0) - \tau_* r(K-1) \tilde{\Psi}(1)\right\},$$

where

$$(C^*_{\mathbb{C}})^1 = C^1([0, 1], X_{\mathbb{C}}).$$

Proof. For any $\tilde{\Psi}$ in $\mathscr{D}(\mathcal{A}^*)$ and Ψ in $\mathscr{D}(\mathcal{A}_0)$, we have

$$\begin{aligned}
\langle\langle\tilde{\Psi}, \mathcal{A}_0\Psi\rangle\rangle &= \langle\tilde{\Psi}(0), (\mathcal{A}_0\Psi)(0)\rangle_1 - \tau_* r(K-1)\int_{-1}^{0}\langle\tilde{\Psi}(s+1), (\mathcal{A}_0\Psi)(s)\rangle_1 ds \\
&= \langle\tilde{\Psi}(0), \dot{\Psi}(0)\rangle_1 - \tau_* r(K-1)\int_{-1}^{0}\langle\tilde{\Psi}(s+1), \dot{\Psi}(s)\rangle_1 ds \\
&= \langle\tilde{\Psi}(0), d\tau_*\Delta\Psi(0) - \alpha\tau_*\nabla\Psi(0) - \tau_* r(K-1)\Psi(-1)\rangle_1 \\
&- \tau_* r(K-1)\int_{-1}^{0}\langle\tilde{\Psi}(s+1), \dot{\Psi}(s)\rangle_1 ds \\
&= \langle\tilde{\Psi}(0), d\tau_*\Delta\Psi(0) - \alpha\tau_*\nabla\Psi(0)\rangle_1 - \tau_* r(K-1)\langle\tilde{\Psi}(0), \Psi(-1)\rangle_1 \\
&- \tau_* r(K-1)\int_{-1}^{0}\langle\tilde{\Psi}(s+1), \dot{\Psi}(s)\rangle_1 ds \\
&= \langle\tilde{\Psi}(0), d\tau_*\Delta\Psi(0) - \alpha\tau_*\nabla\Psi(0)\rangle_1 - \tau_* r(K-1)\langle\tilde{\Psi}(0), \Psi(-1)\rangle_1 \\
&- \tau_* r(K-1)\big[\langle\tilde{\Psi}(s+1), \Psi(s)\rangle_1\big]\Big|_{-1}^{0} + \tau_* r(K-1)\int_{-1}^{0}\langle\dot{\tilde{\Psi}}(s+1), \Psi(s)\rangle_1 ds \\
&= \langle d\tau_*\Delta\tilde{\Psi}(0) - \alpha\tau_*\nabla\tilde{\Psi}(0), \Psi(0)\rangle_1 - \tau_* r(K-1)\langle\tilde{\Psi}(1), \Psi(0)\rangle_1 \\
&+ \tau_* r(K-1)\int_{-1}^{0}\langle\dot{\tilde{\Psi}}(s+1), \Psi(s)\rangle_1 ds \\
&= \langle-\dot{\tilde{\Psi}}(0), \Psi(0)\rangle_1 - \tau_* r(K-1)\int_{-1}^{0}\langle\mathcal{A}^*\tilde{\Psi}(s+1), \Psi(s)\rangle_1 ds \\
&= \langle\langle\mathcal{A}^*\tilde{\Psi}, \Psi\rangle\rangle.
\end{aligned}$$

This completes the proof. □

According to Lemma 2.7, the operator $\mathcal{A}_0$ possesses a unique pair of simple purely imaginary eigenvalues $\pm i\omega_1\tau_*$, and their corresponding eigenfunctions are $\varphi_1 e^{i\omega_1\tau_*\theta}$ and $\varphi_1 e^{-i\omega_1\tau_*\theta}$ for $\theta \in [-1, 0]$. Similarly, $\mathcal{A}^*$ has a pair of eigenvalues $\pm i\omega_1\tau_*$, and the eigenfunctions are $\varphi_1 e^{-i\omega_1\tau_* s}$ and $\varphi_1 e^{i\omega_1\tau_* s}$ for $s \in [0, 1]$. Thus, $P_c = span\{p(\theta), \overline{p(\theta)}\}$ forms the center subspace of Eq (3.1), with $p(\theta)$ defined as $\varphi_1 e^{i\omega_1\tau_*\theta}$. Correspondingly, P^* forms the formal adjoint subspace of P_c under the bilinear form (3.4), with $q(s) = \varphi_1 e^{-i\omega_1\tau_* s}$. Denote $\Phi = (p(\theta), \overline{p(\theta)})$, $\Psi = \frac{1}{M}(q(s), \overline{q(s)})^T$, where

$$M = \frac{L}{2}[1 - \tau r(K-1)e^{-i\omega_1\tau_*}],$$

such that $\langle\langle\Psi, \Phi\rangle\rangle = I_{2\times 2}$.

After performing spectral decomposition of the space B_s with respect to the spectrum $\{\pm i\omega_1\tau_*\}$ as

$$\mathrm{B}_s = P_c \oplus P^*, \tag{3.5}$$

we can then compute the center manifold $\mathscr{C}_0$ of System (3.1).

Let U_t satisfying Eq (3.1). According to Eq (3.5), we decompose U_t as

$$U_t(\theta) = p(\theta)z + \overline{p(\theta)}\bar{z} + C(t, \theta),$$

where $C(t,\theta) \in P^*$ and $z(t) = \langle q(\theta), U_t(\theta)\rangle_1$. Obviously, $C(t,\theta) = U_t(\theta) - 2\mathrm{Re}\{p(\theta)z\}$. By virtue of the center manifold theorem, we express $C(t,\theta)$ on $\mathscr{C}_0$ in the following form in a neighborhood of $(0,0)$:

$$C(z,\bar{z}) = C_{20}(\theta)\frac{z^2}{2} + C_{11}(\theta)z\bar{z} + C_{02}(\theta)\frac{\bar{z}^2}{2} + O(|z|^3). \tag{3.6}$$

Then, Eq (3.3) could be transformed into a differential equation of the variable z, and $z(t)$ satisfies

$$\dot{z}(t) = \frac{\mathrm{d}}{\mathrm{d}t}\langle\langle q(s), U_t\rangle\rangle.$$

Based on the definition of (3.4), we can derive

$$\dot{z}(t) = \mathrm{i}\omega_1\tau_* z(t) + \tfrac{1}{M}\Big\langle q(0), F(\Phi(z(t),\bar{z}(t))^T + c(z(t),\bar{z}(t)), 0)\Big\rangle_1. \tag{3.7}$$

To simplify the presentation, denote

$$G(z,\bar{z}) := \tfrac{1}{M}\Big\langle q(0), F(\Phi(z(t),\bar{z}(t))^T + c(z(t),\bar{z}(t)), 0)\Big\rangle_1; \tag{3.8}$$

then, Eq (3.7) reads

$$\dot{z}(t) = \mathrm{i}\omega_1\tau_* z(t) + G(z,\bar{z}), \tag{3.9}$$

with $G(z,\bar{z}) = G_{20}\frac{z^2}{2} + G_{11}z\bar{z} + G_{02}\frac{\bar{z}^2}{2} + G_{21}\frac{z^2\bar{z}}{2} + \cdots$.

Using Eq (3.8), we obtain the coefficients of G as follows:

$$\begin{aligned}
G_{20} &= -\frac{2}{M}\cdot\frac{r(2K-1)\tau_* e^{-\mathrm{i}\omega_1\tau_*}}{K}\cdot\int_0^L e^{-\frac{\alpha}{d}x}\varphi_1^3(x)dx,\\
G_{11} &= -\frac{1}{M}\cdot\frac{r(2K-1)\tau_*(e^{-\mathrm{i}\omega_1\tau_*} + e^{\mathrm{i}\omega_1\tau_*})}{K}\int_0^L e^{-\frac{\alpha}{d}x}\varphi_1^3(x)dx,\\
G_{02} &= -\frac{2}{M}\cdot\frac{r(2K-1)\tau_* e^{\mathrm{i}\omega_1\tau_*}}{K}\int_0^L e^{-\frac{\alpha}{d}x}\varphi_1^3(x)dx,\\
G_{21} &= -\frac{2}{M}\cdot\frac{r\tau_*}{K}(2e^{-\mathrm{i}\omega_1\tau_*} + e^{\mathrm{i}\omega_1\tau_*})\int_0^L e^{-\frac{\alpha}{d}x}\varphi_1^4(x)dx - \frac{2}{M}\cdot\frac{r(2K-1)\tau_*}{K}\times\\
&\quad\int_0^L [\frac{C_{20}(-1)}{2} + C_{11}(-1) + \frac{C_{20}(0)}{2}e^{\mathrm{i}\omega_1\tau_*} + C_{11}(0)e^{-\mathrm{i}\omega_1\tau_*}]\cdot e^{-\frac{\alpha}{d}x}\varphi_1^3(x)dx,
\end{aligned} \tag{3.10}$$

where $C_{20}(\theta)$ and $C_{11}(\theta)$ are to be determined. It should be noted that $C(z(t),\bar{z}(t))$ is governed by the equation

$$\begin{aligned}
\dot{C} &= \mathscr{A}_0 C + X_0 F(\Phi(z,\bar{z})^T + C(z,\bar{z}), 0)\\
&\quad - \Phi\langle\langle\Psi, X_0 F(\Phi_I(z,\bar{z})^T + C(z,\bar{z}), 0)\rangle\rangle\\
&= \mathscr{A}_0 C + h_{20}\frac{z^2}{2} + h_{11}z\bar{z} + h_{02}\frac{\bar{z}^2}{2} + O(|z|^3),
\end{aligned} \tag{3.11}$$

where the coefficients h_{20}, h_{11}, and h_{02} are determined from

$$\begin{aligned}
&X_0 F(\Phi(z,\bar{z})^T + C(z,\bar{z}), 0) - \Phi\langle\langle\Psi, X_0 F(\Phi(z,\bar{z})^T + C(z,\bar{z}), 0)\rangle\rangle\\
&= h_{20}\frac{z^2}{2} + h_{11}z\bar{z} + h_{02}\frac{\bar{z}^2}{2} + O(|z|^3).
\end{aligned}$$

The application of the chain rule obtains

$$\dot{C} = \frac{\partial C(z,\overline{z})}{\partial z}\dot{z} + \frac{\partial C(z,\overline{z})}{\partial \overline{z}}\dot{\overline{z}}.$$

Thus,

$$\begin{cases} (2\mathrm{i}\omega_1\tau_* - \mathcal{A}_0)C_{20} = h_{20}, \\ -\mathcal{A}_0 C_{11} = h_{11}. \end{cases} \tag{3.12}$$

For $\theta \in [-1, 0)$, the expressions for h_{20} and h_{21} are given by

$$\begin{aligned} h_{20}(\theta) &= -(G_{20}p(\theta) + \overline{G}_{02}\overline{p}(\theta)), \\ h_{11}(\theta) &= -(G_{11}p(\theta) + \overline{G}_{11}\overline{p}(\theta)). \end{aligned} \tag{3.13}$$

On the basis of Eqs (3.12) and (3.13), c_{20} and c_{11} are given by the following forms:

$$C_{11}(\theta) = \frac{\mathrm{i}\overline{G}_{11}}{\omega_1\tau_*}\overline{p}(\theta) - \frac{\mathrm{i}G_{11}}{\omega_1\tau_*}p(\theta) + F. \tag{3.14}$$

$$C_{20}(\theta) = \frac{\mathrm{i}\overline{G}_{02}}{3\omega_1\tau_*}\overline{p}(\theta) + \frac{\mathrm{i}G_{20}}{\omega_1\tau_*}p(\theta) + Ee^{2\mathrm{i}\omega_1\tau_*\theta}. \tag{3.15}$$

Since

$$h_{20}(0) = -\left[\overline{G}_{02}\overline{p}(0) + G_{20}p(0)\right] - 2\tau_* e^{-\mathrm{i}\omega_1\tau_*} r(K-1)\varphi_1(x),$$

from Eq (3.11) and (3.12) with $\theta = 0$, we know that

$$(2\mathrm{i}\omega_1\tau_* - \mathcal{A}_0)Ee^{2\mathrm{i}\omega_1\tau_*\theta}\Big|_{\theta=0} = -2\tau_* e^{-\mathrm{i}\omega_1\tau_*} r(K-1)\varphi_1(x),$$

that is,

$$\mathfrak{L}(2\mathrm{i}\omega_1, \tau_*)E = 2\tau_* e^{-\mathrm{i}\omega_1\tau_*} r(K-1)\varphi_1(x).$$

Then, we can obtain

$$E = 2r(K-1)e^{-\mathrm{i}\omega_1\tau_*}\mathfrak{L}(2\mathrm{i}\omega_1, \tau_*)^{-1}\varphi_1(x). \tag{3.16}$$

Similarly, we can get

$$F = r(K-1)\left(e^{-\mathrm{i}\omega_1\tau_*} + e^{\mathrm{i}\omega_1\tau_*}\right)\mathfrak{L}(0, \tau_*)^{-1}\varphi_1(x). \tag{3.17}$$

In Eqs (3.16) and (3.17), the linear operator $\mathfrak{L}(\mu, \tau)$ is defined as follows:

$$\mathfrak{L}(\mu, \tau)\varphi := d\Delta\varphi - \alpha\varphi_x - r(k-1)\varphi e^{\mu\tau} - \mu\varphi.$$

Then, two key values, μ_2 and β_2, are calculated as follows:

$$\begin{aligned} c_2(0) &= \frac{G_{21}}{2} + \frac{1}{2\omega_1\tau_*}\left(\mathrm{i}G_{11}G_{20} - 2\mathrm{i}|G_{11}|^2 - \mathrm{i}\frac{|G_{02}|^2}{3}\right), \\ \nu_2 &= -\frac{\mathrm{Re}(c_2(0))}{\mathrm{Re}(\lambda'(\tau_*))}, \\ \beta_2 &= 2\mathrm{Re}(c_2(0)). \end{aligned} \tag{3.18}$$

It is well-established that the sign of ν_2 determines the bifurcation direction: $\nu_2 > 0 (< 0)$ corresponds to a forward (backward) bifurcation. The resulting periodic solutions are orbitally stable if $\beta_2 < 0$, and unstable if $\beta_2 > 0$. These solutions emerge when $\tau > \tau_*$ for the forward case and $\tau < \tau_*$ for the backward case. For the specific implications of each parameter involved in the normal form, one can cite [28] for details.

4. Numerical simulations

4.1. Simulation tools and numerical methods

The numerical simulations were performed in MATLAB 2024a by using a finite-difference method. We discretized the spatial interval $[0, L]$ uniformly with mesh size $\Delta x = L/M$ and $M = 40$, and the time interval with step size $\Delta t = 0.0001$. For the interior grid points, the diffusion term was approximated by the standard second-order central difference, and the advection term was approximated by a backward upwind difference. The delay term was computed by the method of steps through the stored values of the solution at the previous $N = \tau/\Delta t$ time levels. Hence, the numerical approximation for the interior nodes takes the form

$$\begin{aligned} u(i, j+1) =& u(i, j) + \Delta t \left[d \frac{u(i+1, j) - 2u(i, j) + u(i-1, j)}{(\Delta x)^2} - \alpha \frac{u(i, j) - u(i-1, j)}{\Delta x} \right] \\ &+ \Delta t \left[r\, u(i, j)(u(i, j) - 1) \left(1 - \frac{u(i, j-N)}{K} \right) \right]. \end{aligned}$$

The left boundary condition was discretized according to

$$u(1, j+1) = \frac{d\, u(2, j+1) + \alpha K \Delta x}{d + \alpha \Delta x},$$

and the right boundary value was fixed by $u(M+1, j+1) = K$. The initial history function was chosen as a small perturbation of the steady state,

$$u_0(x, t) = K + 0.01\,[1 - \cos(2\pi x/L)], \qquad t \in [-\tau, 0].$$

This numerical setting was used to generate the spatiotemporal profiles shown in Figures 2–5.

4.2. Simulations

To validate the theoretical conclusions, numerical computations are carried out in this section. We emphasize that System (1.1) is studied in a nondimensional form, since the Allee threshold has been rescaled to 1. Hence, the parameter values used in this section are not meant to be species-specific fitted data. Instead, they should be understood as biologically meaningful parameter regimes that are used to illustrate the qualitative dynamical behaviors predicted by the theoretical analysis, such as the stability of the positive steady state, the onset of Hopf bifurcation, and the stabilizing role of advection. The parameters in Model (1.1) are assigned as follows:

$$\textbf{(P1)} \quad r = 1, K = 4, d = 0.5, \alpha = 2,\ L = 8.$$

According to (2.6), we can get that

$$\mu_1 \approx 2.0684,\ \mu_2 \approx 2.2748,\ \mu_3 \approx 2.6211,\ \mu_4 \approx 3.1117, \ldots$$

In addition, we obtain $\mu_1 < r(K-1)$, so that (H_1) holds, and we get $n_0 = 4$ from Theorem 2.3. Thus, we have

$$\begin{aligned} &\omega_1 \approx 2.1792,\ \omega_2 \approx 1.9559,\ \omega_3 \approx 1.4594, \\ &\tau_1^{(0)} \approx 1.0729,\ \tau_2^{(0)} \approx 1.2431,\ \tau_3^{(0)} \approx 1.8045. \end{aligned}$$

Clearly, $\tau_* = \tau_1^{(0)} \approx 1.0729$. Furthermore, by using the formula deduced in (3.18), we compute

$$c_2(0) = (-1.2150 + 4.3080\mathrm{i}) \times 10^{14},\ \nu_2 = 2.0687 \times 10^{13},\ \beta_2 = -2.4299 \times 10^{14}.$$

By Theorem 2.8, we know that under the parameters chosen in **(P1)**, $u_* = K$ is stable for $\tau \in [0, 1.0729)$; see Figure 2. Meanwhile, Model (1.1) exhibits a Hopf singularity at $u = K$ when $\tau = \tau_* \approx 1.0729$. Since $\nu_2 > 0$, and $\beta_2 < 0$, the Hopf bifurcation is forward and exists for $\tau > \tau_*$, and the bifurcating periodic solutions are stable when τ is greater than τ_* and sufficiently close to τ_*; see Figure 3.

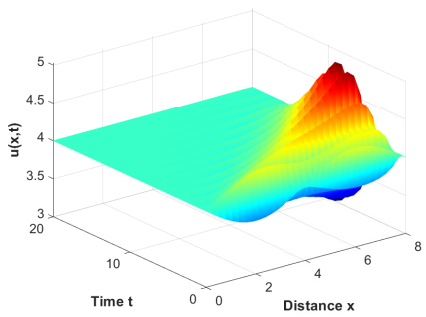

(a) Three-dimensional view of $u(x, t)$.

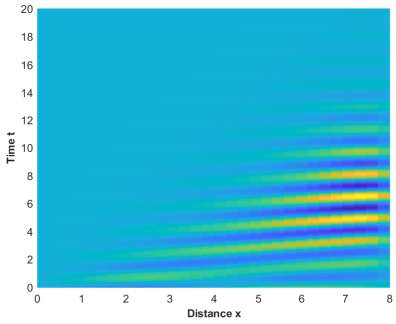

(b) Top-down view of $u(x, t)$.

Figure 2. $u = K$ is stable for $\tau \in [0, 1.0729)$, where $\tau = 0.5 < \tau_*$. The initial value is $u_0(x, t) = K + 0.01 \times [1 - \cos(2\pi x/L)]$, the parameters are given in **(P1)**.

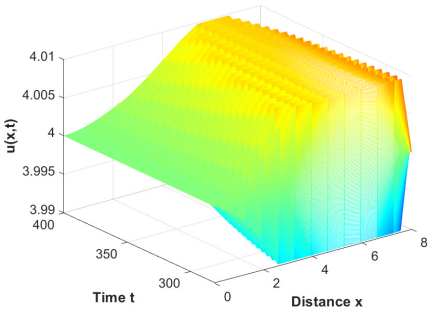

(a) Three-dimensional view of $u(x, t)$.

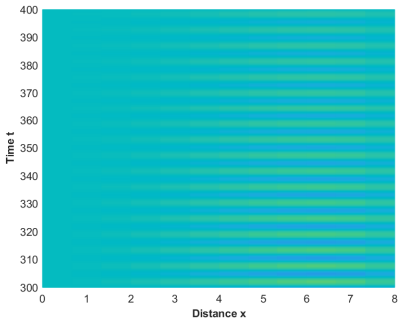

(b) Top-down view of $u(x, t)$.

Figure 3. A periodic solution bifurcated from the positive steady state $u = K$ is stable for $\tau = 1.2$. The initial value is $u_0(x, t) = K + 0.01 \times [1 - \cos(2\pi x/L)]$, and the parameters are given in **(P1)**.

To further illustrate the analytical prediction given by the normal form coefficient β_2, we numerically construct a one-dimensional bifurcation diagram with respect to the delay parameter τ. For several fixed τ, System (1.1) is solved by the finite-difference scheme described above until the transient part decays. The oscillation amplitude is measured by $A(\tau) = \max_{t\in[T_1,T_2]} \|u(\cdot, t) - K\|_\infty$, where $[T_1, T_2]$

is a sufficiently large time window after removing the transient dynamics. Figure 4 shows that the equilibrium $u_* = K$ is stable for $\tau < \tau_*$, corresponding to $A(\tau) = 0$. When τ passes through τ_*, a branch of small-amplitude periodic solutions emerges for $\tau > \tau_*$, and the amplitude increases continuously as τ increases. This numerical result is consistent with the theoretical conclusion that the Hopf bifurcation is supercritical, as indicated by $\nu_2 > 0$ and $\beta_2 < 0$.

When parameters in Model (1.1) are chosen as (**P2**) $r = 1, K = 4, d = 0.5, \alpha = 4,\ L = 8$, we can get that $\mu_1 \approx 8.0684 > r(K-1)$. According to Theorem 2.3, $u = K$ is asymptotically stable for $\tau > 0$; see Figure 5.

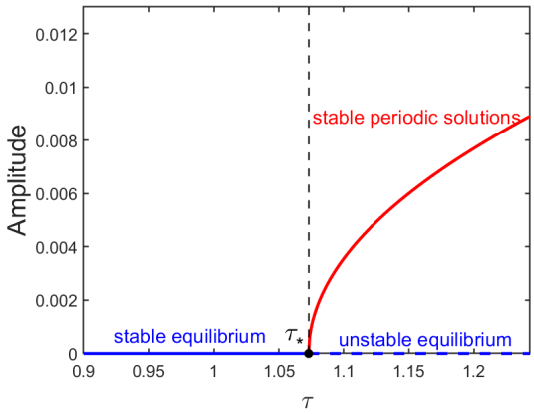

Figure 4. One-dimensional numerical bifurcation diagram with respect to τ; the parameters are given in **(P1).**

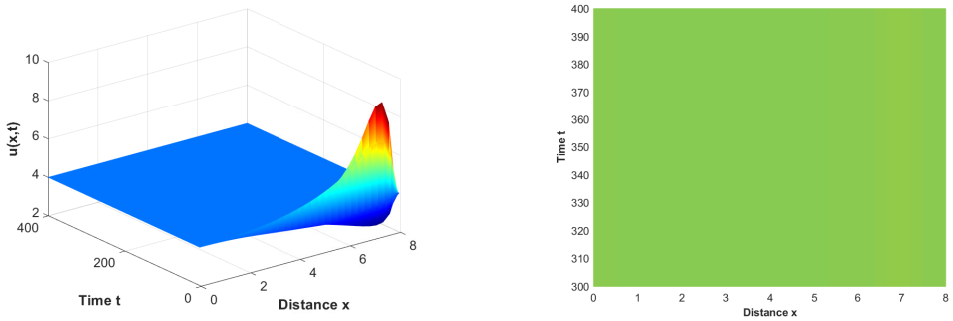

(a) Three-dimensional view of $u(x,t)$.

(b) Top-down view of $u(x,t)$.

Figure 5. The positive steady state $u = K$ which is stable for $\tau = 2.5$. The initial value is $u_0(x,t) = K + 0.01 \times [1 - \cos(2\pi x/L)]$; the parameters are given in **(P2)**.

5. Conclusions

This paper studies a delayed diffusion-advection model for population dynamics which incorporates the strong Allee effect. The model considers a bounded spatial region $(0, L)$ and constant boundary values. This study examines the effect of the advection rate on the dynamics of this model. The results

indicate that the equilibrium remains stable at larger advection rates, whereas it becomes unstable when the advection rate is sufficiently small.

Ecologically, the stabilizing effect of advection can be interpreted as follows. Populations with a strong Allee effect are particularly sensitive to low density, because densities below the Allee threshold may lead to negative growth and hence, to oscillatory or extinction dynamics. In this paper, advection describes directional movement along an environmental gradient. Combined with the source boundary at $x = L$, such movement tends to connect low-density regions with a persistently replenished high-density boundary, thereby reducing prolonged residence below the Allee threshold. Consequently, the delayed negative feedback is less likely to generate sustained oscillations, and the positive equilibrium is more easily stabilized when the advection rate becomes larger. This phenomenon is specific to the current model, but it suggests that directional movement may play a spatially stabilizing role in population models.

Under the condition of a smaller advection rate, the existence of a Hopf singularity is examined by adopting a delay as the bifurcation parameter. To investigate the dynamical properties of the model near the Hopf singularity, we calculate the normal form near the Hopf singularity and provide the detailed formulas. During the derivation of the normal form, a weighted inner product is crucial for constructing the orthonormal basis in the space. Furthermore, a defined formal duality is also important for constructing the formal adjoint operator.

The normal form analysis developed in this work can be extended to advection-diffusion models with other types of boundary conditions. The strong Allee effect model usually exhibits rich dynamical behavior. In our model, constant boundary conditions are adopted, which can be interpreted as a human intervention strategy for population management: When the population density at the boundary is low, it is replenished; when it becomes excessively high, it is reduced. Lastly, numerical simulations were conducted for validation.

This study focuses on the delayed population model with a strong Allee effect and advection. The proposed analytical framework for stability analysis and Hopf bifurcation detection (taking delay as the bifurcation parameter) can be extended to other dynamical systems. For instance, in the fields of reaction kinetics and chemical oscillators, many systems involve diffusion-advection coupling and time delay effects, where the stability and bifurcation analysis are also key issues. Our research methods and conclusions can provide a reference for the analysis of such systems, which will be the focus of our future work.

This work also suggests several other promising directions for future research. Although the system does not exhibit Turing-Hopf bifurcation, Hopf-Hopf bifurcation, or Bogdanov-Takens bifurcation when d and τ are chosen as two varying parameters, the Bautin bifurcation may still exist. Moreover, when other pairs of varying parameters are considered, the existence of these codimension-two bifurcations remains worthy of further investigation in the future. By introducing environmental noise terms into the advection-diffusion equations under study, the properties of stochastic equations can be investigated. Furthermore, when considering interactions such as interspecific competition, predation, or mutualism would extend the research from a one-dimensional advection-diffusion model to a higher-dimensional framework. What's more, replacing simple discrete delays with nonlocal or distributed delays in the model would more realistically capture the feedback effects in biological processes, which is expected to reveal richer bifurcation structures and spatiotemporal dynamics in the system.

Author contributions

Yuying Liu: Conceptualization, Methodology, Software, Formal analysis, Investigation, Writing-original draft, Visualization; Xin Wei: Validation, Resources, Writing-review and editing, Supervision. All authors have read and agreed to the published version of the manuscript.

Use of Generative-AI tools declaration

The authors declare that they have not used Artificial Intelligence (AI) tools in the creation of this article.

Acknowledgments

The authors thank the anonymous referees for their very helpful comments which greatly improve the manuscript. This research is supported by the National Natural Science Foundations of China (No.12301643) and the Natural Science Foundation of Jiangsu Province, China (No. BK20221106).

Conflict of interest

Authors declare no conflicts of interest in this paper.

References

1. K. R. Zenger, B. J. Richardson, A. M. Vachot-Griffin, A rapid population expansion retains genetic diversity within European rabbits in Australia, *Molecular Ecol.*, **12** (2003), 789–794. https://doi.org/10.1046/j.1365-294X.2003.01759.x
2. C. M. King, Pandora's box down-under: Origins and numbers of mustelids transported to New Zealand for biological control of rabbits, *Biol. Invasions*, **19** (2017), 1811–1823. https://doi.org/10.1007/s10530-017-1392-6
3. W. C. Allee, *Animal Aggregations: A Study in General Sociology*, Chicago: University of Chicago Press, 1931.
4. M. A. Lewis, S. V. Petrovskii, R. Potts, *The Mathematics Behind Biological Invasions*, Switzerland: Springer International Publishing, 2016.
5. F. Courchamp, L. Berec, J. Gascoigne, *Allee Effect in Ecology and Conservation*, New York: Oxford University Press, 2008.
6. M. Jankovic, S. Petrovskii, Are time delays always destabilizing? revisiting the role of time delays and the Allee effect, *Theor. Ecol.*, **7** (2014), 335–349. https://doi.org/10.1007/s12080-014-0222-z
7. J. Wang, J. Shi, J. Wei, Dynamics and pattern formation in a diffusive predator prey system with strong Allee effect in prey, *J. Differ. Equ.*, **251** (2011), 1276–1304. https://doi.org/10.1016/j.jde.2011.03.004

8. S. Mandal, F. A. Basir, S. Ray, Additive Allee effect of top predator in a mathematical model of three species food chain, *Energ. Ecol. Environ.*, **6** (2021), 451–461. https://doi.org/10.1007/s40974-020-00200-3

9. Y. Liu, J. Wei, Double Hopf bifurcation of a diffusive predator-prey system with strong Allee effect and two delays, *Nonlinear Anal. Model. Control*, **26** (2021), 72–92. https://doi.org/10.15388/namc.2021.26.20561

10. X. Y. Meng, J. Li, Dynamical behavior of a delayed prey-predator-scavenger system with fear effect and linear harvesting, *Int. J. Biomath.*, **14** (2021), 2150024. https://doi.org/10.1142/S1793524521500248

11. T. Gao, X. Y. Meng, Stability and Hopf bifurcation of a delayed diffusive phytoplankton-zooplankton-fish model with refuge and two functional responses, *AIMS Math.*, **8** (2023), 8867–8901. https://doi.org/10.3934/math.2023445

12. S. X. Wu, X. Y. Meng, Hopf bifurcation analysis of a multiple delays stage-structure predator-prey model with refuge and cooperation, *Electron. Res. Arch.*, **33** (2025), 995–1036. https://doi.org/10.3934/era.2025045

13. S. Devi, R. Fatma, Diffusion-driven instability and bifurcation in the predator-prey system with Allee effect in prey and predator harvesting, *Int. J. Appl. Comput. Math.*, **10** (2024), 39. https://doi.org/10.1007/s40819-023-01673-6

14. S. Chen, J. Wei, X. Zhang, Bifurcation analysis for a delayed diffusive logistic population model in the advective heterogeneous environment, *J. Dynam. Differ. Equat.*, **32** (2020), 823–847. https://doi.org/10.1007/s10884-019-09739-0

15. Z. Li, B. Dai, X. Zou, Stability and bifurcation of a reaction-diffusion-advection model with nonlinear boundary condition, *J. Differ. Equ.*, **363** (2023), 1–66. https://doi.org/10.1016/j.jde.2023.03.015

16. Y. Lou, F. Lutscher, Evolution of dispersal in open advective environments, *J. Math. Biol.*, **69** (2014), 1319–1342. https://doi.org/10.1007/s00285-013-0730-2

17. M. Y. Li, H. Shu, Global dynamics of a mathematical model for HTLV-I infection of $CD4^+$ T cells with delayed CTL response, *Nonlinear Anal.-Real World Appl.*, **13** (2012), 1080–1092. https://doi.org/10.1016/j.nonrwa.2011.02.026

18. L. Yuan, S. Zheng, Z. Alam, Dynamics analysis and cryptographic application of fractional logistic map, *Nonlinear Dyn.*, **96** (2019), 615–636. https://doi.org/10.1007/s11071-019-04810-3

19. S. Chen, J. Shi, Stability and Hopf bifurcation in a diffusive logistic population model with nonlocal delay effect, *J. Differ. Equ.*, **253** (2012), 3440–3470. https://doi.org/10.1016/j.jde.2012.08.031

20. X. P. Yan, C. H. Zhang, Properties of Hopf bifurcation to a reaction-diffusion population model with nonlocal delayed effect, *J. Differ. Equ.*, **385** (2024), 155–182. https://doi.org/10.1016/j.jde.2023.12.006

21. W. Ou, C. Xu, Q. Cui, Y. Pang, Z. Liu, J. Shen, et al., Hopf bifurcation exploration and control technique in a predator-prey system incorporating delay, *AIMS Math.*, **9** (2024), 1622–1651. https://doi.org/doi/10.3934/math.2024080

22. A. Tassaddiq, R. Ahmed, J. Khan, Y. Lee, Impact of double Allee effect on the dynamics and stability of a predator-prey model, *AIMS Math.*, **11** (2026), 1117–1144. https://doi.org/10.3934/math.2026048

23. D. Duan, B. Niu, J. Wei, Hopf-Hopf bifurcation and chaotic attractors in a delayed diffusive predator-prey model with fear effect, *Chaos Soliton Fract.*, **123** (2019), 206–216. https://doi.org/10.1016/j.chaos.2019.04.012

24. Y. Ma, R. Yang, Hopf-Hopf bifurcation in a predator-prey model with nonlocal competition and refuge in prey, *Discrete Contin. Dyn. Syst.-B.*, **29** (2024), 2582–2609. https://doi.org/10.3934/dcdsb.2023193

25. Y. Song, T. Zhang, Y. Peng, Turing-Hopf bifurcation in the reaction-diffusion equations and its applications, *Commun. Nonlinear Sci. Numer. Simul.*, **33** (2016), 229–258. https://doi.org/10.1016/j.cnsns.2015.10.002

26. H. Y. Alfifi, Stability analysis and Hopf bifurcation for two-species reaction-diffusion-advection competition systems with two time delays, *Appl. Math. Comput.*, **474** (2024), 128684. https://doi.org/10.1016/j.amc.2024.128684

27. C. Li, S. Guo, Bifurcation and stability of a reaction-diffusion-advection model with nonlocal delay effect and nonlinear boundary condition, *Nonlinear Anal.-Real World Appl.*, **78** (2024), 104089. https://doi.org/10.1016/j.nonrwa.2024.104089

28. T. Faria, L. T. Magalhaes, Normal forms for retarded functional differential equations with parameters and applications to Hopf Bifurcation, *J. Differ. Equ.*, **122** (1995), 181–200. https://doi.org/10.1006/jdeq.1995.1144

29. S. Guo, J. Wu, *Bifurcation Theory of Functional Differential Equations*, New York: Springer, 2013.

30. J. Guckenheimer, P. Holmes, *Nonlinear Oscillations, Dynamical Systems, and Bifurcations of Vector Fields*, New York: Springer, 1983.

AIMS Press